THE JOURNAL OF BIOLOGICAL CHEMISTRY VOL. 289, NO. 8, pp. 5061–5073, February 21, 2014

Rod Visual Pigment Optimizes Active State to Achieve Efficient G Protein Activation as Compared with Cone Visual Pigments*

Received for publication, August 6, 2013, and in revised form, December 24, 2013 Published, JBC Papers in Press, December 27, 2013, DOI 10.1074/jbc.M113.508507

Keiichi Kojima, Yasushi Imamoto, Ryo Maeda, Takahiro Yamashita, and Yoshinori Shichida[1]

From the Department of Biophysics, Graduate School of Science, Kyoto University, Kyoto 606-8502, Japan

Background: The relationship between the properties of visual pigment and photoreceptor amplification efficiency is controversial.
Results: Rhodopsin activates G protein more efficiently than cone pigments.
Conclusion: Visual pigment properties are directly related to the photoreceptor sensitivity diversification.
Significance: Amplification of cell responses is regulated by receptor molecules.

Most vertebrate retinas contain two types of photoreceptor cells, rods and cones, which show different photoresponses to mediate scotopic and photopic vision, respectively. These cells contain different types of visual pigments, rhodopsin and cone visual pigments, respectively, but little is known about the molecular properties of cone visual pigments under physiological conditions, making it difficult to link the molecular properties of rhodopsin and cone visual pigments with the differences in photoresponse between rods and cones. Here we prepared bovine and mouse rhodopsin (bvRh and mRh) and chicken and mouse green-sensitive cone visual pigments (cG and mG) embedded in nanodiscs and applied time-resolved fluorescence spectroscopy to compare their G_t activation efficiencies. Rhodopsin exhibited greater G_t activation efficiencies than cone visual pigments. Especially, the G_t activation efficiency of mRh was about 2.5-fold greater than that of mG at 37 °C, which is consistent with our previous electrophysiological data of knock-in mice. Although the active state (Meta-II) was in equilibrium with inactive states (Meta-I and Meta-III), quantitative determination of Meta-II in the equilibrium showed that the G_t activation efficiency per Meta-II of bvRh was also greater than those of cG and mG. These results indicated that efficient G_t activation by rhodopsin, resulting from an optimized active state of rhodopsin, is one of the causes of the high amplification efficiency of rods.

Most vertebrate retinas contain two types of photoreceptor cells, rods and cones, which are responsible for scotopic and photopic vision, respectively. Rods are more sensitive to light than cones, whereas cones display a more rapid photoresponse and rapid adaptation than rods (1, 2). Despite the striking difference in photoresponses between rods and cones, accumulated evidence indicates that both cells have a similar signal transduction cascade, suggesting that the differences in photoresponse between rods and cones could originate from differences in the molecular properties and concentrations of transduction proteins (2–5). Therefore, whether or not the properties of rod and cone visual pigments are directly related to the photoresponse of rods and cones has been a long-standing issue.

A visual pigment is a photoreceptor molecule that contains 11-*cis*-retinal as its chromophore. The role of a visual pigment is to absorb a photon and activate G protein (6). Thus, if a visual pigment efficiently absorbs a photon and efficiently activates G protein, the photosensitivity of the photoreceptor cell is high. To elucidate the contribution of rod and cone visual pigments to the photoresponse of photoreceptor cells, we have produced knock-in mice whose rods express mouse green-sensitive cone visual pigment (mG)[2] instead of rhodopsin (7). Electrophysiological assays showed that rods containing mG have amplification efficiency about one-third that of wild-type rods. Because the amplification efficiency of the transduction cascade per bleached pigment in mouse rods was about 6.8-fold higher than that in mouse cones (8), the electrophysiological assay results implied that about half of the difference in amplification efficiency between rods and cones is derived from the difference of visual pigments (7, 8).

It has been reported previously that the G_t activation efficiencies of rhodopsin and cone visual pigments were similar to each other based on experiments performed at about 0 °C (7, 9, 10), although those of rhodopsin and cone visual pigments of a poikilothermic animal (carp) were recently reported to be different at 20 °C (11, 12). Thus, it is likely that the difference in amplification efficiency between wild-type rods and rods con-

---

* This work was supported by Japanese Ministry of Education, Culture, Sports, Science, and Technology Grants-in-aid for Scientific Research 23370070 (to Y. I.), 25440167 (to T. Y.), and 25251036 (to Y. S.) and grants for excellent graduate schools.

[1] To whom correspondence should be addressed. Tel.: 81-75-753-4213; Fax: 81-75-753-4210; E-mail: shichida@rh.biophys.kyoto-u.ac.jp.

[2] The abbreviations used are: mG, mouse green-sensitive cone visual pigment; GTPγS, guanosine 5–3-*O*-(thio)triphosphate; ROS, rod outer segment; G_t, transducin; POPC, 1-palmitoyl-2-oleoyl-*sn*-glycero-3-phosphocholine; POPG, 1-palmitoyl-2-oleoyl-*sn*-glycero-3-phospho-(1′-*rac*-glycerol); DOPC, 1,2-dioleoyl-phosphatidylcholine; DM, *n*-dodecyl β-D-maltoside; Meta-I, Meta-II, and Meta-III, bleaching intermediates of cone visual pigments corresponding to metarhodopsin I, metarhodopsin II, and metarhodopsin III, respectively; bvRh, bovine rhodopsin; mRh, mouse rhodopsin; cG, chicken green-sensitive cone visual pigment; MSP, membrane scaffold protein; SVD, singular value decomposition; MII, Meta-II.

taining mG is caused by temperature-dependent intrinsic properties of visual pigments such as the thermal equilibrium between active state Meta-II and its precursor Meta-I and/or the lifetime of Meta-II that may compete with the deactivation process consisting of phosphorylation by rhodopsin kinase (7). Regarding the latter possibility, Shi *et al.* (13) reported that the response profile of mouse rods containing mouse UV cone pigment differed depending on whether rod arrestin was present or absent, although the effect of arrestin was not very strong. Of course, that finding does not rule out the possibility that the G_t activation efficiencies of rhodopsin and cone visual pigments are different at physiological temperature (37 °C) due to different temperature dependence of the G_t activation efficiency between rhodopsin and cone visual pigments.

Because the decay of the active state of cone visual pigments at 37 °C was expected to be too fast to permit measurement of G_t activation efficiency by conventional biochemical assays, we considered it desirable to prepare cone visual pigment samples whose environment would be similar to that of the photoreceptor cell membranes and that could be subjected to spectroscopic measurements with high time resolution. For this purpose, we used nanodiscs to prepare the samples.

Nanodiscs are soluble membrane particles that consist of phospholipids and membrane scaffold protein(s) (MSPs) (14, 15) into which membrane proteins such as G protein-coupled receptors can be inserted (16–18). It has been reported that rhodopsin in nanodiscs effectively activated G_t (19) and was inactivated by GRK1 and visual arrestin (20, 21) and that β_2-adrenergic receptor in nanodiscs effectively activated G_s (22). These findings indicate that spectroscopic assays using nanodisc samples are an alternative to biochemical assays using native membranes or liposomes.

In this study, we prepared nanodisc samples containing bvRh, mRh, cG, and mG. Cone visual pigments are phylogenetically classified into four groups, the S (SWS1), M1 (SWS2), M2 (RH2), and L (LWS) groups (23–25). Among them, the M2 and L groups are phylogenetically the closest to and farthest from the rhodopsin group (RH group), respectively, and we therefore selected cG from the M2 group and mG from the L group for the present analyses.

We confirmed that nanodiscs mimic the native membrane environment and compared the G_t activation efficiencies of photoactivated bvRh, mRh, cG, and mG. Then, using the ratios of Meta-II at equilibrium determined from time-resolved spectroscopic measurements, we calculated the G_t activation efficiency per Meta-II. From these results, the contribution of G_t activation efficiency to the photoresponses of rods and cones and the mechanism giving rise to the different G_t activation efficiencies between rhodopsin and cone visual pigments are discussed.

EXPERIMENTAL PROCEDURES

Preparation of Pigments—Bovine rod outer segments (ROSs) were isolated from fresh bovine retina as described previously (26). Recombinant bvRh, mRh, cG, and mG were transiently expressed in HEK293T cell lines as reported previously (27). The cDNAs of cG and mG were tagged by the epitope sequence of the monoclonal antibody Rho1D4 (ETSQVAPA) at the C terminus. The transfected cells were collected by centrifugation and suspended in Buffer A (50 mM HEPES, 140 mM NaCl, pH 6.5), and 11-*cis*-retinal was added to the cell suspension to reconstitute photoactive pigments. The cells were solubilized with Buffer B (0.75% CHAPS, 50 mM HEPES, 140 mM NaCl, 3 mM $MgCl_2$, pH 7.5) and adsorbed to an Rho1D4 affinity column (27, 28). After the column was washed with Buffer B containing phospholipids (a mixture of 0.78 mM POPC and 0.52 mM POPG, 1.3 mM POPC, or a mixture of 0.78 mM DOPC and 0.52 mM POPG), the pigment was eluted by the addition of the synthetic peptide having the epitope sequence. To obtain purified bvRh in DM suspension, the transfected cells were solubilized with Buffer C (50 mM HEPES, 140 mM NaCl, 3 mM $MgCl_2$, pH 7.5) containing 1% DM and adsorbed to an Rho1D4 affinity column. After washing with Buffer C containing 0.02% DM, bvRh was eluted by addition of the peptide.

Preparation of Nanodiscs—MSP1E3D1 was used as the MSP of nanodiscs. It was expressed in *Escherichia coli* and purified as described previously (14). MSP was quantitated by absorbance at 280 nm (29910 $\text{M}^{-1}\ \text{cm}^{-1}$). MSP was mixed with phospholipids (POPC/POPG, POPC, or DOPC/POPG in Buffer B) and purified recombinant pigment at a molar ratio of 750:10:1 (lipids:MSP:pigment) to prepare nanodiscs containing monomeric pigment (20, 29). The mixture was dialyzed against Buffer D (140 mM Tris/HCl, 50 mM NaCl, 5 mM EDTA, pH 7.4) at 4 °C to reconstitute the nanodiscs by removing detergent. The aggregates and liposomes were removed from the mixture using a Superdex 200 column. The collected fractions containing nanodiscs were further purified by Rho1D4 affinity column chromatography in Buffer C to remove the empty nanodiscs.

Spectroscopic Measurements—Absorption spectra of the samples were recorded using a UV-visible spectrophotometer (Shimadzu UV-2450 and UV-2400). The temperature of the samples was kept at 0 °C by using a cell holder equipped with a circulation system for the temperature-controlled water. Time-resolved absorption spectra were recorded using a high speed charge-coupled device spectrophotometer (C10000 System, Hamamatsu Photonics) (27, 30). This spectrophotometer continuously acquires full spectra (2048 channels) with a wavelength resolution of about 0.5 nm at time intervals of 0.2 ms. For spectroscopic measurements, ROSs and nanodiscs were suspended in Buffer C. The sample temperature was maintained by using a cell holder equipped with a Peltier device. The samples were irradiated with a neodymium-doped yttrium aluminum garnet laser at 532 nm (Minilite-II, Continuum) 100 ms after the measurements were started.

Analysis of Time-resolved Spectroscopic Data—The spectral changes were analyzed by singular value decomposition (SVD) and global fitting methods by using the software Igor Pro (WaveMetrics Inc.) (27, 31). The difference spectra after photoexcitation were arranged in matrix *A*. Its columns and rows correspond to absorbance *versus* wavelength and absorbance *versus* time after photoexcitation, respectively. The SVD calculation decomposed *A* into a product of a left singular matrix *U*, a diagonal matrix containing singular values *S*, and a transpose of a right singular matrix *V* as follows.

$$A = U \times S \times V^T \qquad \text{(Eq. 1)}$$

We determined the number of columns considered in the following estimation (n) from the number of significant singular values and basis spectra in matrices U and V.

$$A = U \times S \times V^T \approx U_n \times S_n \times V_n^T \qquad \text{(Eq. 2)}$$

where U_n and V_n^T contain n columns and S_n contains n singular values. Assuming that all the transitions from one intermediate to another are first-order reactions, V_n^T was fitted with the sum of exponential functions as follows.

$$V_n^T = C \times (\exp(-k_1 t_i), \exp(-k_2 t_i), \cdots, \exp(-k_{n-1} t_i), 1)^T \qquad \text{(Eq. 3)}$$

Matrix C contains amplification factors of exponential function $(\exp(-k_j t_i))$, and t_i is the time after photon absorption at which the ith spectrum was measured. From Equations 1–3, matrix A can be expressed as follows.

$$A \approx U_n \times S_n \times C \times (\exp(-k_1 t_i), \exp(-k_2 t_i), \cdots, \exp(-k_{n-1} t_i), 1)^T \qquad \text{(Eq. 4)}$$

The jth column of $U_n \times S_n \times C$ is the b-spectrum that represents the kinetic component with rate constant k_j. The nth column of the $U_n \times S_n \times C$ is the b0 spectrum that corresponds to the constant spectrum at infinite time. In this study, the opposite-signed b-spectra are shown except for b0.

Preparation of Bovine Rod G_t—Bovine rod G_t was purified from bovine retina as described previously (32). The concentration of G_t was estimated by the Bradford assay. Purified G_t was stored in Buffer C.

G_t Activation Assay and Estimation of Initial Velocities—G_t activation was measured using fluorescence assays. Fluorescence changes of intrinsic Trp of G_t were monitored using a laboratory-constructed photon counting system with some modifications (30). Briefly, the excitation beam was generated using a Jasco J-600 spectropolarimeter. Fluorescence was detected using a photon counting head (H7360-01, Hamamatsu Photonics) connected to the controller unit (C8855, Hamamatsu Photonics). Fluorescence greater than 310 nm was collected using an optical filter (U-360) in front of the photon counting head. Counting duration was 100 ms. The pigments were irradiated with a yellow flash generated by a combination of a short arc xenon flash lamp (SA-200F, Nissin Electronic) and a Y-52 filter.

G_t activation efficiency was evaluated using the initial velocities as described previously (30). For bvRh and mRh, the initial slopes of the fluorescence increase in the presence and absence of G_t were calculated, and then the initial velocity of fluorescence increase due to G_t activation ($V_0^{F(G_t \to G_{t^*})}$) was obtained by subtracting the latter from the former.

On the other hand, although Meta-II of cG and mG decays into opsin during G_t activation (Scheme 1), $V_0^{F(G_t \to G_{t^*})}$ was analyzed based on Michaelis-Menten kinetics as follows (30). In Scheme 1, concentration changes of G_t, Meta-II, Meta-II·G_t, and opsin are expressed as follows.

$$\frac{d[G_t^*]}{dt} = k_{cat} \times [\text{Meta-II·}G_t] \qquad \text{(Eq. 5)}$$

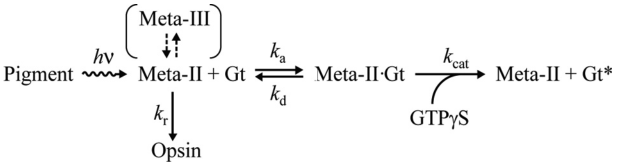

SCHEME 1. **Michaelis-Menten model for G_t activation by photoactivated pigments.**

$$\frac{d[\text{Meta-II}]}{dt} = -(k_r + k_a[G_t])[\text{Meta-II}] + (k_d + k_{cat})[\text{Meta-II·}G_t] \qquad \text{(Eq. 6)}$$

$$\frac{d[\text{Meta-II·}G_t]}{dt} = k_a[G_t][\text{Meta-II}] - (k_d + k_{cat})[\text{Meta-II·}G_t] \qquad \text{(Eq. 7)}$$

$$\frac{d[\text{Opsin}]}{dt} = k_r[\text{Meta-II}] \qquad \text{(Eq. 8)}$$

Because the total amount of Meta-II, Meta-II·G_t, and opsin is constant, Equation 9 can be solved as follows.

$$[\text{Meta-II}]_{t=0}^{\text{total}} = [\text{Meta-II}] + [\text{Meta-II·}G_t] + [\text{Opsin}] \qquad \text{(Eq. 9)}$$

In the present experimental conditions, Meta-II of cone visual pigments rapidly decays before the depletion of G_t. Assuming that the concentration of G_t is constant, these differential equations (Equations 5–9) can be solved as follows.

$$[\text{Meta-II·}G_t] = [\text{Meta-II}]_{t=0}^{\text{total}} \times \frac{k_a[G_t]}{(-k_r' + k_r'')}(\exp(-k_r' t) - \exp(-k_r'' t)) \qquad \text{(Eq. 10)}$$

$$[\text{Opsin}] = [\text{Meta-II}]_{t=0}^{\text{total}} \times \left\{ \frac{(k_r'' - k_r)}{-k_r' + k_r''}(1 - \exp(-k_r' t)) - \frac{(k_r' - k_r)}{-k_r' + k_r''}(1 - \exp(-k_r'' t)) \right\} \qquad \text{(Eq. 11)}$$

where k_r' and k_r'' are the apparent rate constants expressed as follows.

$$k_r', k_r'' = \frac{(k_r + k_a[G_t] + k_d + k_{cat})}{2} \mp \frac{\sqrt{(k_r + k_a[G_t] + k_d + k_{cat})^2 - 4(k_d + k_{cat})k_r}}{2} \qquad \text{(Eq. 12)}$$

The rate of G_t activation is obtained from Equations 5, 10, and 12.

$$\frac{d[G_t^*]}{dt} = \frac{k_{cat}[\text{Meta-II}]_{t=0}^{\text{total}} \times k_a[G_t]}{\sqrt{(k_r + k_a[G_t] + k_d + k_{cat})^2 - 4(k_d + k_{cat})k_r}} \times (\exp(-k_r' t) - \exp(-k_r'' t)) \qquad \text{(Eq. 13)}$$

Therefore, the concentration of G_t^* is expressed as follows.

$$[\mathrm{G_t}^*] = \frac{k_{\mathrm{cat}}[\text{Meta-II}]^{\mathrm{total}}_{t=0} \times k_a[\mathrm{G_t}]}{\sqrt{(k_r + k_a[\mathrm{G_t}] + k_d + k_{\mathrm{cat}})^2 - 4(k_d + k_{\mathrm{cat}})k_r}} \times \left(\frac{1}{k_r'}\left(1 - \exp(-k_r't) - \frac{1}{k_r''}(1 - \exp(-k_r''t)\right)\right) \quad \text{(Eq. 14)}$$

The concentration of opsin is expressed as follows using Equations 11 and 12.

$$[\mathrm{Opsin}] = [\text{Meta-II}]^{\mathrm{total}}_{t=0} \times \frac{\{(k_r'' - k_r)(1 - \exp(-k_r't)) - (k_r' - k_r)(1 - \exp(-k_r''t))\}}{\sqrt{(k_r + k_a[\mathrm{G_t}] + k_d + k_{\mathrm{cat}})^2 - 4(k_d + k_{\mathrm{cat}})k_r}} \quad \text{(Eq. 15)}$$

Here we considered two cases in which Meta-II decay is much slower than the association and dissociation of Meta-II·G$_t$ ($k_r \ll k_a[\mathrm{G_t}]$, k_d, k_{cat}) (*i.e.* cG) and in which Meta-II decay is comparable with the association and dissociation of Meta-II·G$_t$ (k_{cat}, $k_d \ll k_a[\mathrm{G_t}]$, k_r) (*i.e.* mG). If $k_r \ll k_a[\mathrm{G_t}]$, k_d, and k_{cat}, Equation 12 shows that $k_r' \ll k_r''$ and $k_r'' \approx k_a[\mathrm{G_t}] + k_d + k_{\mathrm{cat}}$. Therefore, the fast component $(1/k_r''(1 - \exp(-k_r''t)))$ in Equations 14 and 15 is not observable because the present time resolution (100 ms) is lower than k_r''. Thus, Equations 13 and 15 become Equations 16 and 17.

$$\frac{d[\mathrm{G_t}^*]}{dt} \approx \frac{k_{\mathrm{cat}}[\text{Meta-II}]^{\mathrm{total}}_{t=0} \times [\mathrm{G_t}]}{[\mathrm{G_t}] + K}\exp(-k_r't),\ K = \frac{k_d + k_{\mathrm{cat}}}{k_a} \quad \text{(Eq. 16)}$$

$$[\mathrm{Opsin}] \approx [\text{Meta-II}]^{\mathrm{total}}_{t=0} \times (1 - \exp(-k_r't)) \quad \text{(Eq. 17)}$$

On the other hand, if Meta-II decay is rapid (k_{cat}, $k_d \ll k_a[\mathrm{G_t}]$, k_r), Equation 12 shows that $k_r' \ll k_r''$ and $k_r'' \approx k_a[\mathrm{G_t}] + k_r$. Because Meta-II decay of mG was much faster than the present time resolution (see the legend of Fig. 7), the fast component is not observable.

$$\frac{d[\mathrm{G_t}^*]}{dt} \approx \frac{k_{\mathrm{cat}}[\text{Meta-II}]^{\mathrm{total}}_{t=0} \times [\mathrm{G_t}]}{[\mathrm{G_t}] + K}\exp(-k_r't),\ K = \frac{k_r}{k_a} \quad \text{(Eq. 18)}$$

$$[\mathrm{Opsin}] \approx [\text{Meta-II}]^{\mathrm{total}}_{t=0} \times \frac{k_r + k_a[\mathrm{G_t}](1 - \exp(-k_r't))}{k_r + k_a[\mathrm{G_t}]} \quad \text{(Eq. 19)}$$

Equations 16 and 18 become Equation 20.

$$[\mathrm{G_t}^*] = \frac{k_{\mathrm{cat}}[\text{Meta-II}]^{\mathrm{total}}_{t=0}}{k_r'([\mathrm{G_t}] + K)}(1 - \exp(-k_r't)) \quad \text{(Eq. 20)}$$

Equations 16, 18, and 20 imply that the concentration change of G$_t$*, which is progressively decelerated, is expressed by an exponential function with the apparent rate constant of Meta-II decay (k_r'). Therefore, although fluorescence increases due to both the opsin formation and G$_t$ activation occur for cG and mG, the experimentally obtained fluorescence increase is expressed by single exponential function. Florescence increases at time *t* for opsin formation ($\Delta F_t^{\mathrm{MII}\rightarrow\mathrm{Ops}}$) and G$_t$ activation ($\Delta F_t^{\mathrm{G_t}\rightarrow\mathrm{G_{t^*}}}$) are expressed as follows.

$$\Delta F_t^{\mathrm{G_t}\rightarrow\mathrm{G_{t^*}}} = \Delta F_\infty^{\mathrm{G_t}\rightarrow\mathrm{G_{t^*}}}(1 - \exp(-k_r't)) \quad \text{(Eq. 21)}$$

and

$$\Delta F_t^{\mathrm{MII}\rightarrow\mathrm{Ops}} = \Delta F_\infty^{\mathrm{MII}\rightarrow\mathrm{Ops}}(1 - \exp(-k_r't)),\ (k_r \ll k_a[\mathrm{G_t}], k_d, k_{\mathrm{cat}}) \quad \text{(Eq. 22)}$$

or

$$\Delta F_t^{\mathrm{MII}\rightarrow\mathrm{Ops}} = \Delta F_\infty^{\mathrm{MII}\rightarrow\mathrm{Ops}}\left(\frac{k_r + k_a[\mathrm{G_t}](1 - \exp(-k_r't))}{k_r + k_a[\mathrm{G_t}]}\right),\ (k_{\mathrm{cat}}, k_d \ll k_a[\mathrm{G_t}], k_r) \quad \text{(Eq. 23)}$$

The derivatives of Equations 21–23 are the rates of fluorescence increases for opsin formation ($V_t^{F(\mathrm{MII}\rightarrow\mathrm{Ops})}$) and G$_t$ activation ($V_0^{F(\mathrm{G_t}\rightarrow\mathrm{G_{t^*}})}$).

$$V_t^{F(\mathrm{G_t}\rightarrow\mathrm{G_{t^*}})} = k_r'\Delta F_\infty^{\mathrm{G_t}\rightarrow\mathrm{G_{t^*}}}\exp(-k_r't) \quad \text{(Eq. 24)}$$

and

$$V_t^{F(\mathrm{MII}\rightarrow\mathrm{Ops})} = k_r'\Delta F_\infty^{\mathrm{MII}\rightarrow\mathrm{Ops}}\exp(-k_r't),\ (k_r \ll k_a[\mathrm{G_t}], k_d, k_{\mathrm{cat}}) \quad \text{(Eq. 25)}$$

or

$$V_t^{F(\mathrm{MII}\rightarrow\mathrm{Ops})} = k_r'\Delta F_\infty^{\mathrm{MII}\rightarrow\mathrm{Ops}}\frac{k_a[\mathrm{G_t}]}{k_r + k_a[\mathrm{G_t}]}\exp(-k_r't),\ (k_{\mathrm{cat}}, k_d \ll k_a[\mathrm{G_t}], k_r) \quad \text{(Eq. 26)}$$

Therefore, the initial velocity of G$_t$ activation is calculated as follows.

$$V_0^{F(\mathrm{G_t}\rightarrow\mathrm{G_{t^*}})} = k_r'(\Delta F_\infty^{\mathrm{total}} - \Delta F_\infty^{\mathrm{MII}\rightarrow\mathrm{Ops}}) \quad \text{(Eq. 27)}$$

where $\Delta F_\infty^{\mathrm{total}}$ is given by Equation 28.

$$\Delta F_\infty^{\mathrm{total}} = \Delta F_\infty^{\mathrm{G_t}\rightarrow\mathrm{G_{t^*}}} + \Delta F_\infty^{\mathrm{MII}\rightarrow\mathrm{Ops}} \quad \text{(Eq. 28)}$$

From Equations 16 and 18, the initial velocities of G$_t$ activation are plotted against G$_t$ concentration to estimate V_{max} as follows.

$$V_0^{F(\mathrm{G_t}\rightarrow\mathrm{G_{t^*}})} = \frac{k_{\mathrm{cat}}[\text{Meta-II}]^{\mathrm{total}}_{t=0} \times [\mathrm{G_t}]}{[\mathrm{G_t}] + K} = V_{\mathrm{max}}\frac{[\mathrm{G_t}]}{[\mathrm{G_t}] + K} \quad \text{(Eq. 29)}$$

The concentrations of pigments were 2 or 20 nM in nanodisc samples and 2 nM in ROS samples. The concentrations of GTPγS and G$_t$ were 100 and 200–1200 nM, respectively. G$_t$ activation assays were performed in Buffer C.

RESULTS

Pigments in Nanodiscs—In this study, we successfully inserted rhodopsin and cone visual pigments into nanodiscs using CHAPS buffer containing lipids. POPC consists of a palmitoyl group and an oleyl group, which are major components of bovine ROS phosphatidylcholine (33, 34). Superdex 200 column

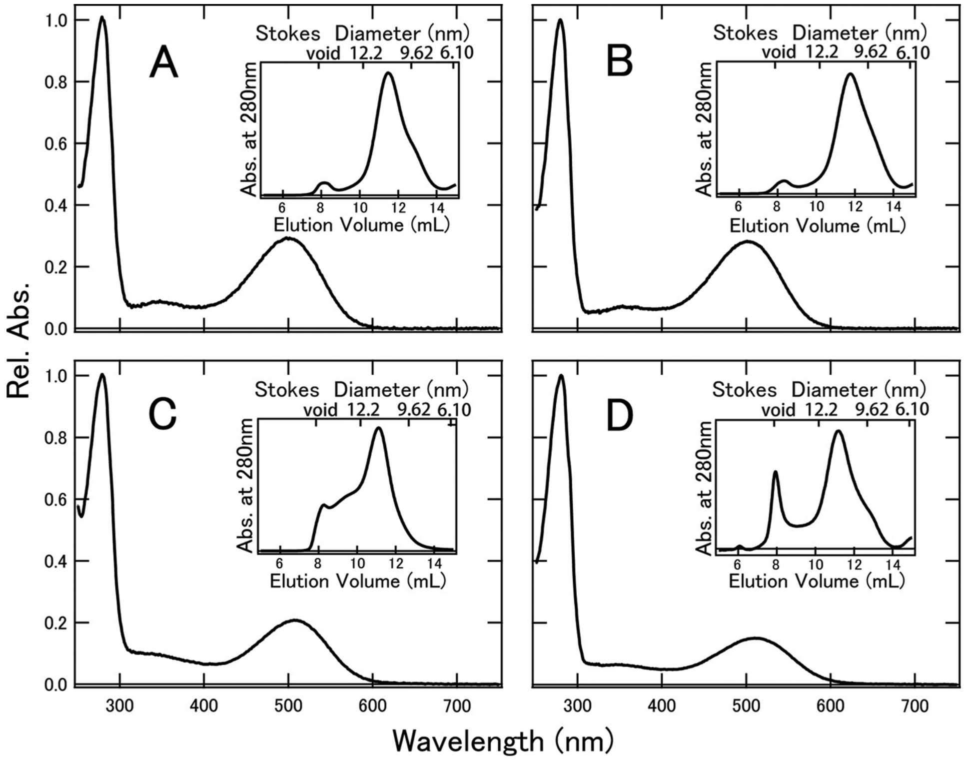

FIGURE 1. **Absorption spectra of bvRh (*A*), mRh (*B*), cG (*C*), and mG (*D*) in POPC/POPG nanodiscs.** The spectra were measured at 0 °C. The *insets* show chromatograms of nanodisc size exclusion. We collected the peak fraction at 10.5–12.5 ml corresponding to the Stokes diameters of nanodiscs containing pigments. *Rel. Abs.*, relative absorbance.

chromatography (Fig. 1, *insets*) demonstrated that the Stokes diameters of nanodiscs containing bvRh, mRh, cG, and mG were 10.7, 10.3, 11.3, and 11.2 nm, respectively, which were in good agreement with previous reports using MSP1E3D1 (14, 20). After column chromatography, bvRh, mRh, cG, and mG in nanodiscs were further purified by Rho1D4 affinity column chromatography. The absorption spectra of these pigments in nanodiscs are shown in Fig. 1. By using the extinction coefficients of bvRh and MSP, the ratio of MSP to bvRh in nanodiscs was estimated to be 2.2–2.3. This shows that nanodiscs contained monomeric rhodopsin under the experimental conditions. The absorption spectra of cG and mG in nanodiscs showed lower absorbances in the visible region (Fig. 1, *C* and *D*), indicating that the extinction coefficients of cG and mG in the ultraviolet region (~280 nm) are relatively larger than those of bvRh and mRh. This is consistent with the fact that cG and mG contain more tryptophan and tyrosine residues than bvRh and mRh (Fig. 1, *A* and *B*).

Comparison of G_t Activation Efficiencies of Rhodopsin and Cone Visual Pigments—Using these rhodopsin and cone visual pigments in nanodiscs, we succeeded in measuring fluorescence changes indicative of G_t activation with high time resolution. Before comparing the G_t activation efficiencies of bvRh, mRh, cG, and mG in nanodiscs, we first measured the G_t activation efficiencies of bvRh in ROSs and in nanodiscs containing POPC/POPG (POPC/POPG nanodiscs) to examine whether nanodiscs are useful for examining G_t activation efficiencies of visual pigments under physiological conditions (Fig. 2, *A* and *B*). Initial velocities of G_t activation were calculated and plotted as a function of G_t concentration and were fitted with the Michaelis-Menten equation to estimate turnover rates of G_t activation by photoactivated pigments (V_{max}/R^*) (Fig. 2*C* and Table 1). Initial velocities and V_{max}/R^* of bvRh in ROSs and nanodiscs were similar, indicating that nanodiscs were useful for estimating G_t activation efficiencies of visual pigments in a membrane environment. Next, we compared the G_t activation efficiencies of bvRh, cG, mRh, and mG in POPC/POPG nanodiscs at 0–37 °C. Typical fluorescence changes are shown in Fig. 3, *A–D*. The calculated initial velocities of G_t activation were fitted with the Michaelis-Menten equation or Equation 29 to estimate V_{max}/R^* (Fig. 4, *A–D*, and Table 1). V_{max}/R^* values of bvRh and mRh were greater than those of cG and mG, indicating that rhodopsin activates G_t more efficiently than cone visual pigments at 0–37 °C. This suggests that rhodopsin activates G_t more efficiently than cone visual pigments under physiological conditions. At 37 °C, V_{max}/R^* of mRh (38.8 G_t^*/s) was about 2.5-fold greater than that of mG (15.4 G_t^*/s). This difference in G_t activation efficiency is consistent with our previous electrophysiological study (7), which showed that the amplification efficiency of mRh was about 3-fold greater than that of mG. Therefore, it is likely that the difference in G_t activation efficiency between rhodopsin and cone visual pigments was the main contributor to the difference in the amplification efficiency of the single photon response in that previous study. Additionally, V_{max}/R^* of cG (21.1 G_t^*/s) was about 1.4-fold greater than that of mG (15.4 G_t^*/s) at 37 °C. This suggests that different subtypes of cone visual pigments have different G_t activation efficiencies. Moreover, we measured G_t activation efficiencies of bvRh and mG in nanodiscs containing POPC and those containing DOPC/POPG (POPC nanodiscs and DOPC/

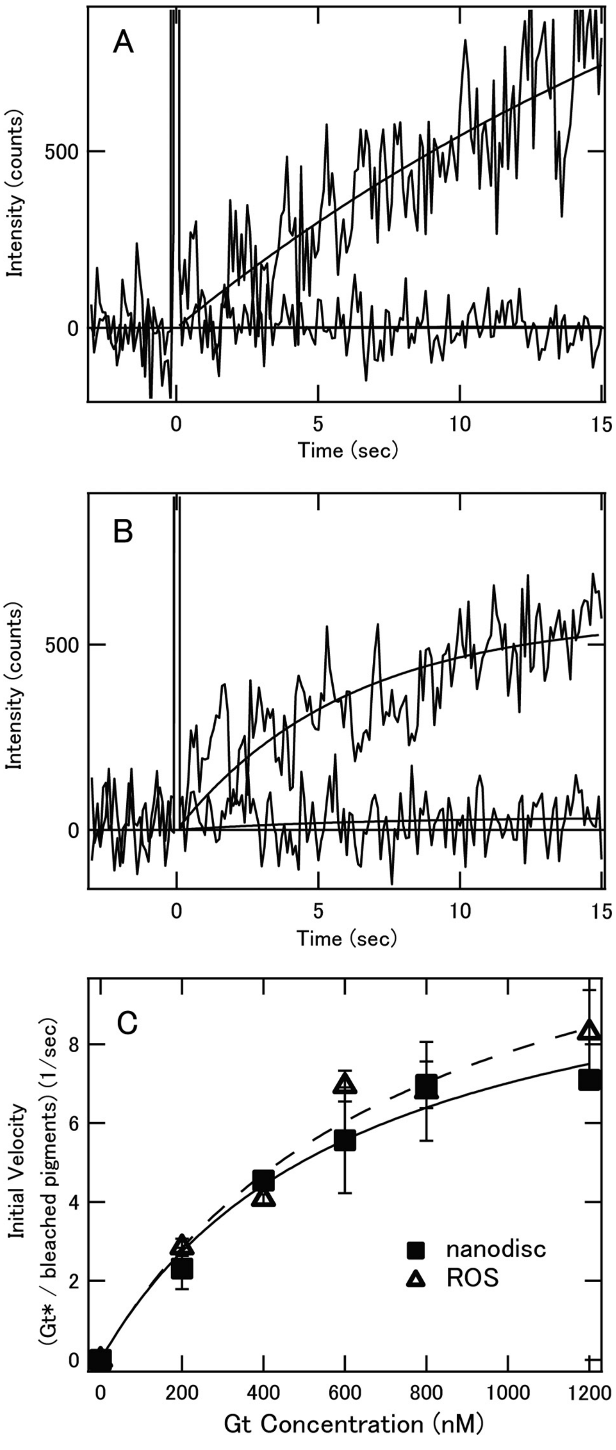

FIGURE 2. **Comparison of G_t activation efficiencies of bvRh in ROSs and nanodiscs.** *A*, G_t activation by photoactivated bvRh in POPC/POPG nanodiscs. 2 nM pigment was mixed with 400 nM G_t and 100 μM GTPγS at 20 °C. The mixture was irradiated with a yellow flash at time 0, and the fluorescence intensity was monitored (*upper* traces). The fluorescence increase that originated from opsin formation was monitored in the absence of G_t at 20 °C (*lower* traces). *B*, G_t activation by photoactivated bvRh in ROSs. 2 nM pigment was mixed with 400 nM G_t and 100 μM GTPγS at 20 °C. The mixture was irradiated with a yellow flash at time 0, and the fluorescence intensity was monitored (*upper* traces). The fluorescence increase that resulted from opsin formation was monitored in the absence of G_t at 20 °C (*lower* traces). *C*, initial velocities of G_t activation by photoactivated bvRh in ROSs and POPC/POPG nanodiscs at 20 °C (*open triangles* and *filled squares*, respectively). Plots of initial velocities were fitted by the Michaelis-Menten equation (*solid line* for ROSs and *dashed line* for nanodiscs). *Error bars* represent S.D. estimated from three independent measurements.

TABLE 1

Kinetic parameters of G_t activation by rhodopsin and cone visual pigments

Values are shown as average ± S.D. calculated from three independent measurements. ND, not determined.

Sample	Temperature	V_{max}/R*	V_{max}/Meta-II	K_m or K
	°C	s^{-1}	s^{-1}	nM
ROS[a]	20	13.8 ± 0.9	24.2 ± 1.5	774 ± 60
bvRh/nanodisc[a]	20	11.9 ± 1.3	23.3 ± 2.5	718 ± 152
bvRh/nanodisc	0	2.42 ± 0.27	17.3 ± 1.9	638 ± 227
	10	5.42 ± 0.98	17.5 ± 3.2	465 ± 117
	20	11.2 ± 1.7	22.0 ± 3.3	595 ± 45
	37	38.6 ± 3.3	52.2 ± 4.5	1158 ± 120
mRh/nanodisc	20	11.3 ± 1.6	ND	731 ± 142
	37	38.8 ± 1.2	ND	856 ± 124
cG/nanodisc	0	1.56 ± 0.21[b]	3.90 ± 0.53[c]	363 ± 108
	10	3.96 ± 0.24[b]	7.62 ± 0.46[c]	841 ± 89
	20	8.21 ± 0.79[b]	13.5 ± 1.3[c]	932 ± 45
	37	21.1 ± 1.9[b]	28.5 ± 2.6[c]	901 ± 130
mG/nanodisc	20	4.73 ± 0.69[b,d]	12.1 ± 1.8[c]	1068 ± 177
	37	15.4 ± 1.2[b,d]	37.6 ± 3.0[c]	794 ± 153

[a] The concentration of bvRh was 2 nM. In other experiments, the concentrations of pigments were 20 nM. Lipid composition of nanodiscs was a mixture of POPC/POPG at a ratio of 3:2 (POPC/POPG).

[b] Significantly different from V_{max}/R* of bvRh and mRh at the same temperature ($p < 0.05$).

[c] Significantly different from V_{max}/Meta-II of bvRh at the same temperature ($p < 0.05$).

[d] Significantly different from V_{max}/R* of cG at the same temperature ($p < 0.05$).

POPG nanodiscs, respectively) to estimate the effect of lipid composition of nanodiscs on the G_t activation efficiency at 37 °C (Fig. 5 and Table 2). V_{max}/R* values of bvRh in POPC and DOPC/POPG nanodiscs were 34.5 and 35.5 G_t*/s, respectively. V_{max}/R* values of mG in POPC and DOPC/POPG nanodiscs were 13.6 and 15.9 G_t*/s, respectively. V_{max}/R* values in POPC and DOPC/POPG nanodiscs were consistent with those in POPC/POPG nanodiscs.

Estimation of Meta-II Ratio in Equilibrium State of bvRh—To estimate the G_t activation efficiencies of Meta-II and characterize the G_t-activating states of rhodopsin and cone visual pigments, we first analyzed the photobleaching processes and estimated the Meta-II ratio in the equilibrium states of bvRh in which the active state was in equilibrium with the inactive state. Spectral changes of bvRh in ROSs, POPC/POPG nanodiscs, and DM suspension after light irradiation were measured. We analyzed the difference spectra by SVD and global fitting and obtained b-spectra (Fig. 6, *A–C*) and time constants (data not shown) for the respective kinetic components. We observed bvRh Meta-II formation (b1 and b2) at 0, 10, and 20 °C and bvRh Meta-II formation (b1) at 37 °C in nanodiscs. Additionally, we also observed Meta-II formation (b1 and b2) of bvRh in ROSs and DM suspension at 20 °C. At 20 °C, the time constants of Meta-II formation for recombinant bvRh in POPC/POPG nanodiscs (6.23 and 47.7 ms) were similar to those of native bvRh in ROSs (8.65 and 37.8 ms), like those of native bvRh in nanodiscs (35). At this time scale, decay of Meta-II was not observed. Therefore, the b0 spectrum, which is the spectrum extrapolated to infinite time, shows the equilibrium between Meta-I and Meta-II (Fig. 6*D*). Using this b0 spectrum, the fraction of Meta-II in Meta-I/Meta-II equilibrium ($F_{Meta\text{-}II}$) was estimated as described previously (36, 37) (Table 3). $F_{Meta\text{-}II}$ in nanodiscs was 51% at 20 °C, which was consistent with that in ROSs (57%), whereas $F_{Meta\text{-}II}$ in DM-solubilized bvRh was 100%, which was considerably higher than $F_{Meta\text{-}II}$ in nanodiscs

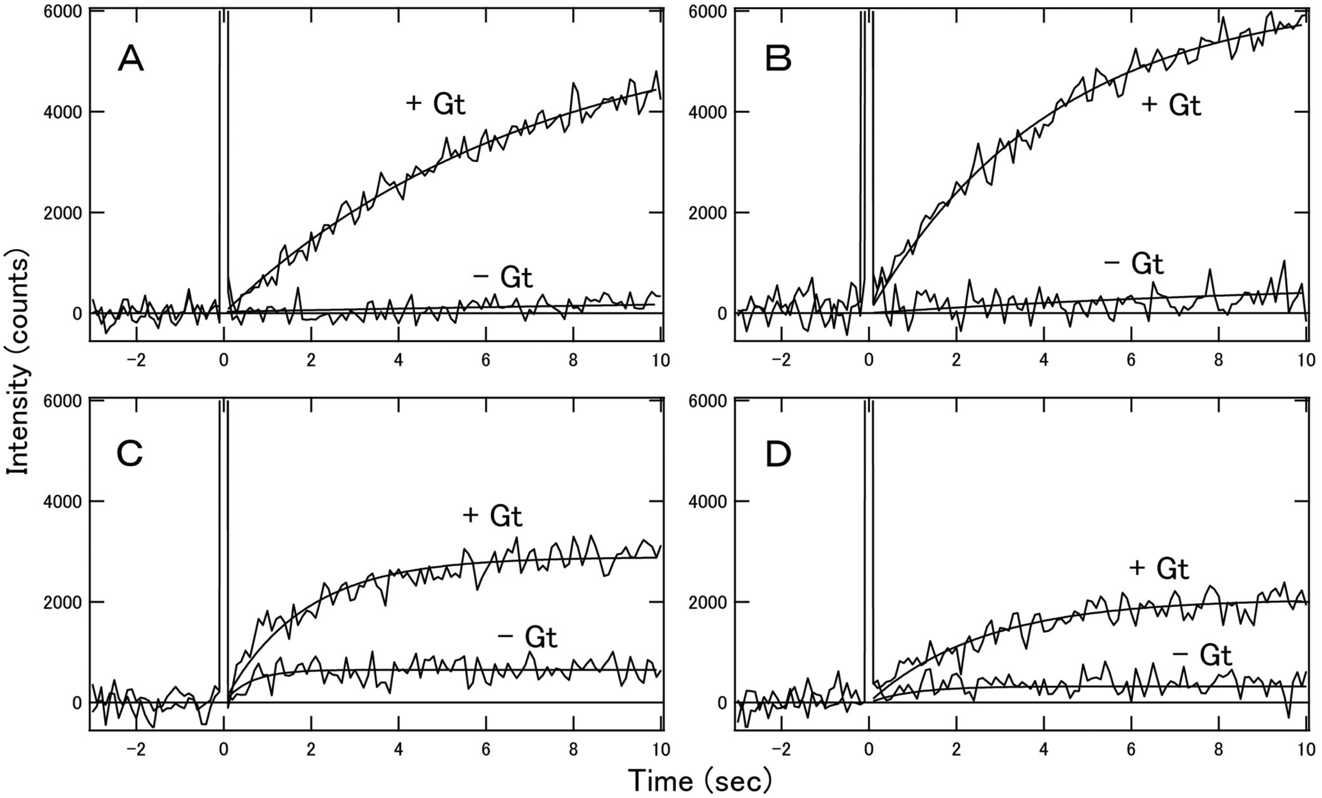

FIGURE 3. **G_t activation by photoactivated bvRh (*A*), mRh (*B*), cG (*C*), and mG (*D*) in POPC/POPG nanodiscs.** 20 nM pigment was mixed with 400 nM G_t and 100 μM GTPγS at 37 °C. The mixture was irradiated with a yellow flash at time 0, and the fluorescence intensity was monitored (*upper* traces). The fluorescence increase that originated from opsin formation was monitored in the absence of G_t at 37 °C (*lower* traces).

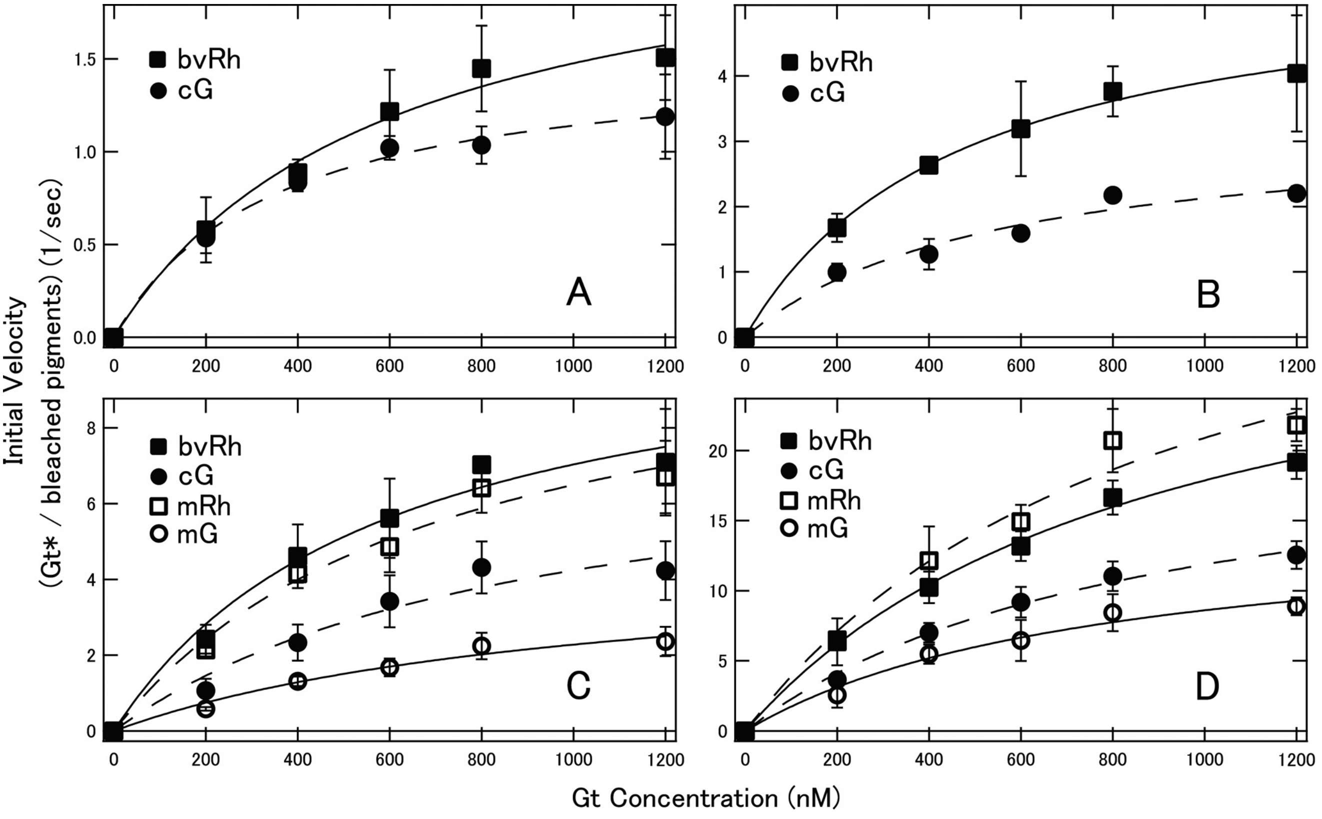

FIGURE 4. **Initial velocities of G_t activation by photoactivated pigments in POPG/POPG nanodiscs.** Initial velocities of bvRh, cG, mRh, and mG (*closed squares*, *closed circles*, *open squares*, and *open circles*, respectively) at 0 (*A*), 10 (*B*), 20 (*C*), and 37 °C (*D*) were plotted against G_t concentration and fitted by the Michaelis-Menten equation or Equation 29 (*solid lines* for bvRh and mG and *dashed lines* for mRh and cG) to estimate V_{max}/R^*. *Error bars* represent S.D. estimated from three independent measurements.

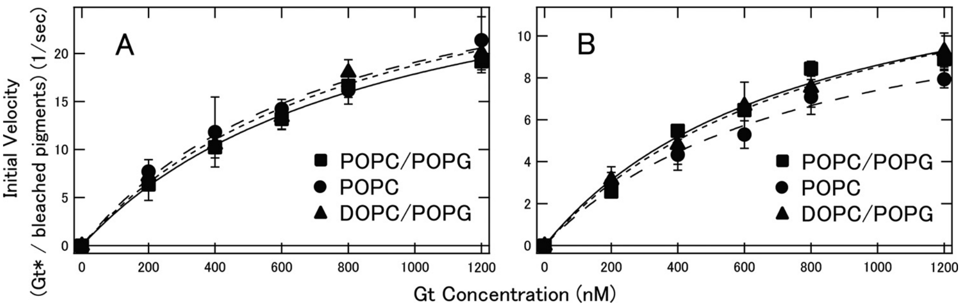

FIGURE 5. **Initial velocities of G_t activation by photoactivated bvRh (*A*) and mG (*B*) in POPC/POPG, POPC, and DOPC/POPG nanodiscs.** Initial velocities of bvRh and mG in POPC/POPG, POPC, and DOPC/POPG nanodiscs (*closed squares*, *closed circles*, and *closed triangles*, respectively) at 37 °C were plotted against G_t concentration and fitted by the Michaelis-Menten equation or Equation 29 (*solid lines* for POPC/POPG nanodiscs, *dashed lines* for POPC nanodiscs, and *dotted lines* for DOPC/POPG nanodiscs) to estimate V_{max}/R*. *Error bars* represent S.D. estimated from three independent measurements.

TABLE 2

Kinetic parameters of G_t activation by rhodopsin and cone visual pigments

Values are shown as average ± S.D. calculated from three independent measurements. The concentrations of pigments were 20 nM. The experiments were performed at 37 °C.

Sample	Lipid	V_{max}/R*	K_m or K
		s^{-1}	nM
bvRh/nanodisc	POPC/POPG	35.3 ± 4.7	994 ± 172
	POPC	34.5 ± 3.8	816 ± 229
	DOPC/POPG	35.5 ± 2.8	897 ± 167
mG/nanodisc	POPC/POPG	15.4 ± 1.2	794 ± 153
	POPC	13.6 ± 1.3	848 ± 292
	DOPC/POPG	15.9 ± 1.0	868 ± 179

and ROSs. The same analysis at various temperatures showed that $F_{\text{Meta-II}}$ was sensitive to temperature (Table 3).

Estimation of Meta-II Ratios in Equilibrium State of cG and mG—We also analyzed the photobleaching processes to estimate the Meta-II ratios of cG and mG in POPC/POPG nanodiscs, although this analysis was more complicated. Spectral changes after photon absorption were measured and analyzed by SVD and global fitting at 0–37 °C. From the SVD analysis, b-spectra (Fig. 7, *A* and *B*) and time constants (data not shown) were obtained. At 0 and 10 °C, we observed Meta-I → Meta-II + Meta-III (b1 and b2 at 0 and 10 °C and b1 at 20 and 37 °C), Meta-II → opsin (b3 at 0 and 10 °C and b2 at 20 and 37 °C), and Meta-III → opsin (b4 at 0 and 10 °C and b3 at 20 and 37 °C) of cG. This is consistent with the photobleaching process of cG in DM suspension (30). On the other hand, we observed Meta-I → Meta-II + Meta-III (b1), Meta-II → opsin (b2), and Meta-III → opsin (b3) of mG at 10–37 °C, which is consistent with the photobleaching process of cG. Then, to estimate the ratios of Meta-I, Meta-II, and Meta-III in the equilibria of these intermediates for cG and mG, we calculated model spectra of these intermediates by using the b-spectra obtained. The model absorption spectrum of the dark state ([Dark]) of cG or mG was constructed using the difference spectra before and after light exposure in the presence of hydroxylamine as reported previously (38).

The model spectra of intermediates of cG and mG were calculated using the model spectra of the dark state and the b-spectra of cG at 0 °C or those of mG at 10 °C. The Meta-I spectrum ([Meta-I]) was calculated as follows.

$$[\text{Meta-I}] = [\text{Dark}] + B_{t=0}/f_d \qquad \text{(Eq. 30)}$$

where f_d is the fraction of the photoactivated pigment and $B_{t=0}$ is the difference spectrum at $t = 0$.

$$B_{t=0} = \text{b0} - \text{b1} - \text{b2} - \text{b3} - \text{b4 (cG)} \qquad \text{(Eq. 31)}$$

$$B_{t=0} = \text{b0} - \text{b1} - \text{b2} - \text{b3 (mG)} \qquad \text{(Eq. 32)}$$

[Meta-III] was calculated as follows.

$$[\text{Meta-III}] = [\text{Dark}] + \text{b0}/f_d - \text{b4}/f_3 \text{ (cG)} \qquad \text{(Eq. 33)}$$

$$[\text{Meta-III}] = [\text{Dark}] + \text{b0}/f_d - \text{b3}/f_3 \text{ (mG)} \qquad \text{(Eq. 34)}$$

where f_3 is the fraction of Meta-III, which was determined such that b0 cancels the absorbance at 380 nm in b4 (cG) or b3 (mG). [Meta-II] was calculated as follows.

$$[\text{Meta-II}] = \left([\text{Meta-I}] - \frac{\text{b1}}{f_2} + \frac{[\text{Meta-I}] - [\text{Meta-III}]}{f_3}\right)/(1 - f_3) \qquad \text{(Eq. 35)}$$

where f_2 is the fraction of Meta-II, which was determined such that b1 cancels the absorbance at 480 nm.

The calculated α-bands of intermediates were fitted by retinoid curves, and β-bands were fitted by Gaussian curves as described previously (38). Fig. 7, *C* and *D*, show the calculated model spectra of the dark state and intermediates of cG and mG, respectively.

The fraction of Meta-III ($F_{\text{Meta-III}}$) was estimated by using b4 spectra for cG at 0 and 10 °C or b3 spectra for cG at 20 and 37 °C and for mG, which reflect the decay of Meta-III, and model spectra of Meta-III (Table 4). We then calculated difference spectra (B_{eq}) obtained when the equilibrium among Meta-I, Meta-II, and Meta-III is formed as follows (Fig. 7, *E* and *F*).

$$B_{eq} = \text{b0} - \text{b3} - \text{b4 (cG at 0 and 10 °C)} \qquad \text{(Eq. 36)}$$

$$B_{eq} = \text{b0} - \text{b2} - \text{b3 (cG at 20 and 37 °C and mG)} \qquad \text{(Eq. 37)}$$

The difference spectra were fitted with the model spectra to estimate the fractions of Meta-I, Meta-II, and Meta-III in the equilibrium (Table 4). The $F_{\text{Meta-II}}$ values of cG and mG were increased at higher temperature, like that of bvRh, although $F_{\text{Meta-II}}$ of mG was smaller than that of cG. At 37 °C, $F_{\text{Meta-II}}$ of bvRh (74%) was similar to that of cG (74%) and greater than that of mG (41%).

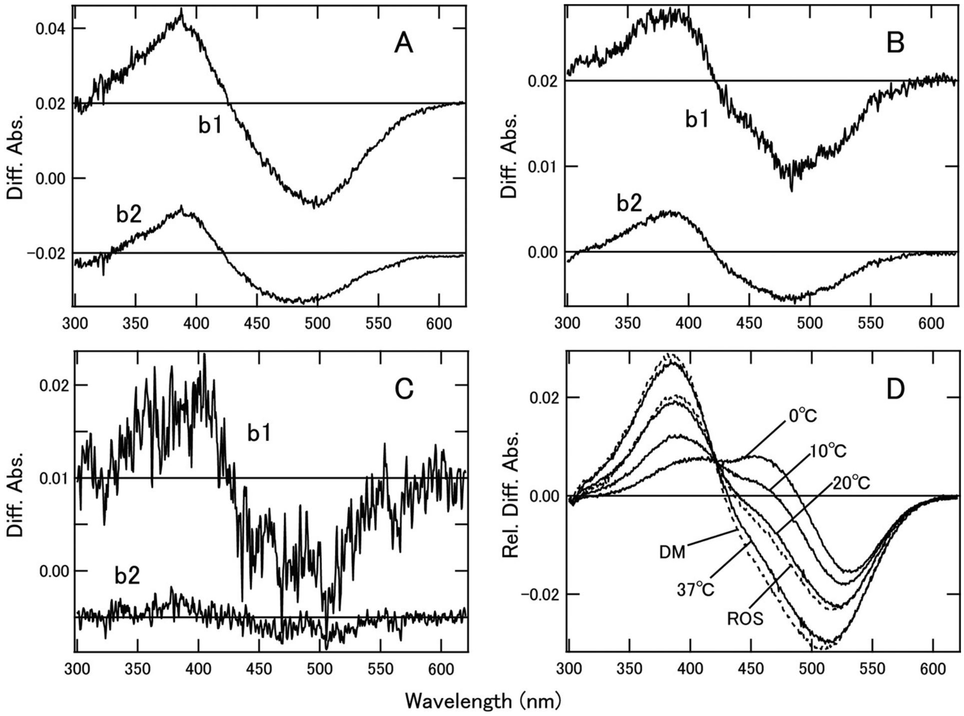

FIGURE 6. **Photobleaching processes and estimation of Meta-II ratios of bvRh.** The b-spectra of bvRh in POPC/POPG nanodiscs at 20 °C (*A*), in ROSs at 20 °C (*B*), and in DM suspension at 20 °C (*C*) calculated by SVD analysis are presented. The b-spectra of bvRh in nanodiscs at 0 and 10 °C were consistent with those at 20 °C. The b1 spectrum of bvRh in nanodiscs at 37 °C was consistent with that at 20 °C. Two-step formation of Meta-II (b1 and b2) is consistent with previous reports that suggested the presence of two forms of Meta-I (Meta-Ia and Meta-Ib) (32, 45). b0 spectra, which were difference spectra in the equilibrium state, of bvRh in nanodiscs and ROSs and DM suspension are shown in *D* (*solid lines* for bvRh in nanodiscs at 0–37 °C and *dashed lines* for bvRh in ROSs or DM suspension at 20 °C). These spectra were fitted by Meta-I and Meta-II model spectra as described previously (36, 37) to estimate $F_{\text{Meta-II}}$ (Table 3). *Diff. Abs.*, difference absorbance; *Rel. Diff. Abs.*, relative difference absorbance.

TABLE 3
Fraction of Meta-II in the equilibrium of rhodopsin

Sample	Temperature	$F_{\text{Meta-II}}$
	°C	%
bvRh/nanodisc	0	14
	10	31
	20	51
	37	74
bvRh/DM	20	100
ROS	20	57

G_t Activation Efficiencies of Meta-II—To compare the nature of the G_t-activating state (Meta-II) generated by photoactivation of rod and cone visual pigments, we estimated the turnover rates of the activation of G_t by Meta-II ($V_{\max}$/MII) of bvRh, cG, and mG using $F_{\text{Meta-II}}$ (Tables 3 and 4) and listed them in Table 1. $V_{\max}$/MII of bvRh in POPC/POPG nanodiscs (22.0 G_t*/s) was consistent with that of bvRh in ROSs (24.2 G_t*/s), like $V_{\max}$/R*. $V_{\max}$/MII of bvRh (52.2 G_t*/s at 37 °C) was greater than $V_{\max}$/MII of cG (28.5 G_t*/s at 37 °C) and mG (37.6 G_t*/s at 37 °C) in POPC/POPG nanodiscs, indicating that rhodopsin forms more efficient G_t-activating states, which finally cause the higher $V_{\max}$/R* of rhodopsin. $V_{\max}$/MII values of bvRh and cG measured at four temperatures (0, 10, 20, and 37 °C) were then plotted in an Arrhenius manner (Fig. 8), and the apparent activation energy (E_a) was calculated to be 38 kJ/mol for cG and 22 kJ/mol for bvRh. $V_{\max}$/MII values of mG measured at 20 and 37 °C were also plotted in Fig. 8, showing that the E_a of mG would be similar to that of cG. These results suggested that E_a of cone visual pigments is about 2-fold greater than that of rhodopsin.

DISCUSSION

In this study, we compared G_t activation efficiencies of rod and cone visual pigments in a membrane environment at physiological temperature with high time resolution using a fluorescence assay (Figs. 2 and 3). Rhodopsin showed about 2–3-fold higher G_t activation efficiencies than cone visual pigments (Figs. 4 and 5 and Tables 1 and 2). Moreover, the specific G_t activation efficiency of Meta-II formed from rhodopsin was higher than that of Meta-II formed from cone visual pigments (Fig. 8).

Nanodiscs Mimic Native Membrane Environments—We confirmed that bvRh in POPC/POPG nanodiscs showed similar properties to bvRh in native ROS membranes (Fig. 2 and Table 1). Our data indicated that $V_{\max}$/R*, $V_{\max}$/MII, and $F_{\text{Meta-II}}$ of photoactivated bvRh in nanodiscs were in good agreement with those of bvRh in ROSs (Tables 1 and 3), which is consistent with previous studies (18, 35). Thus, these results demonstrated that nanodiscs mimic the native membrane environment and that the above mentioned molecular properties of visual pigments in the physiological environment can be studied using nanodisc samples.

G_t Activation Efficiencies of Rhodopsin and Cone Visual Pigments—In this study, we measured the initial velocities of G_t activation at different G_t concentrations at 0–37 °C to estimate the activation efficiencies (turnover rates of photoactivated pigments ($V_{\max}$/R*)) of bvRh, mRh, cG, and mG (Figs. 4 and 5 and Tables 1 and 2) in nanodiscs. Our fluorescence assay showed that $V_{\max}$/R* values of bvRh and mRh were greater than those of

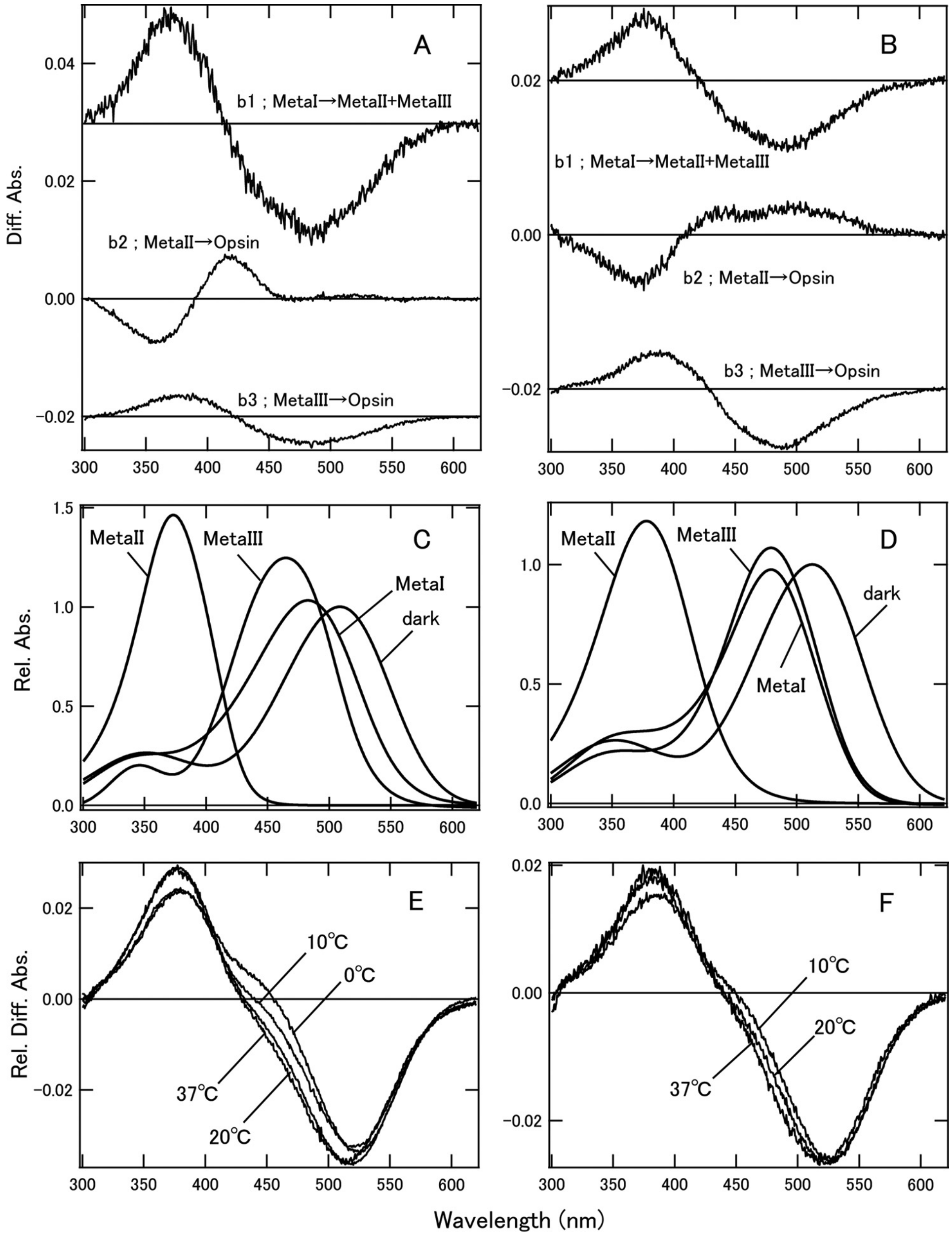

FIGURE 7. **Photobleaching processes and estimation of Meta-II ratios of cG and mG in POPC/POPG nanodiscs.** *A*, b-spectra calculated by SVD analysis of cG in nanodiscs at 20 °C. At 0 and 10 °C, b1 and b2 spectra were consistent with b1 at 20 °C, and b3 and b4 were consistent with b2 and b3, respectively, at 20 °C. At 37 °C, b-spectra were consistent with those at 20 °C. *B*, b-spectra calculated by SVD analysis of mG in nanodiscs at 20 °C. At 10 and 37 °C, the b-spectra were consistent with those at 20 °C. The time constants of b1, b2, and b3 were 4.9 ms, 79 ms, and 4.6 s, respectively, at 20 °C. *C*, model absorption spectra of dark state and photobleaching intermediates of cG. Absorption maxima of cG were 508 nm for dark state, 483 nm for Meta-I, 374 nm for Meta-II, and 465 nm for Meta-III. *D*, model absorption spectra of dark state and photobleaching intermediates of mG. Absorption maxima of mG were 513 nm for dark state, 479 nm for Meta-I, 378 nm for Meta-II, and 479 nm for Meta-III. For details, see the text. *E*, calculated difference spectra (B_{eq}) of equilibrium states of cG at 0–37 °C. These spectra were fitted by model dark state, Meta-I, Meta-II, and Meta-III spectra to estimate $F_{\text{Meta-II}}$ (Table 4). *F*, calculated difference spectra (B_{eq}) in equilibrium states of mG at 10–37 °C. These spectra were also fitted by the model spectra to estimate $F_{\text{Meta-II}}$ (Table 4). *Diff. Abs.*, difference absorbance; *Rel. Diff. Abs.*, relative difference absorbance.

TABLE 4

Fraction of Meta intermediates in the equilibrium of cone visual pigments

Sample	Temperature	$F_{\text{Meta-I}}$	$F_{\text{Meta-II}}$	$F_{\text{Meta-III}}$
	°C	%	%	%
cG/nanodisc	0	52	40	8
	10	38	52	10
	20	31	61	7
	37	15	74	12
mG/nanodisc	10	48	27	25
	20	39	39	22
	37	29	41	30

cG and mG at 0–37 °C. It should be noted that this finding is inconsistent with previous reports showing that the initial velocity of G_t activation by cone visual pigments was similar to that of rhodopsin (7, 9, 10). The previous studies were performed in the presence of about a 10-fold excess of G_t using the pigments in liposomes or native membranes at 0 or 4 °C. We assessed the dependence of V_{max}/R^* on G_t concentration and showed that the initial velocities of cG and bvRh were very similar in the presence of a 10-fold excess of G_t relative to visual pigment (Fig. 4). Our data are also consistent with a recent

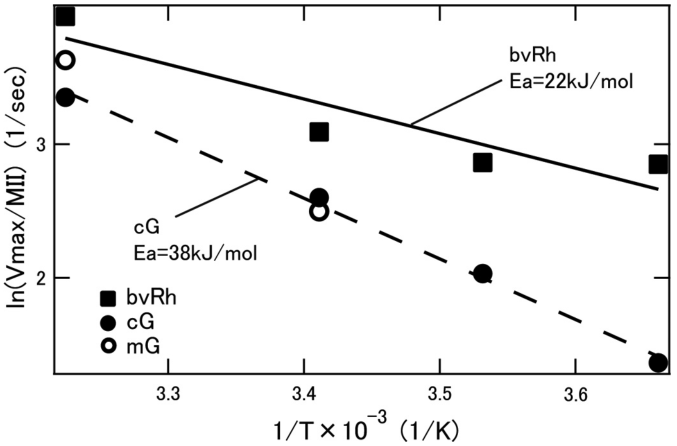

FIGURE 8. **Arrhenius plots of turnover rates (V_{max}/MII) of G_t activation by bvRh, cG, and mG (*closed squares*, *closed circles*, and *open circles*, respectively) in POPC/POPG nanodiscs.** Plots of bvRh and cG were fitted by *straight lines* (*solid* and *dashed lines*, respectively) to calculate apparent activation energy (E_a).

report that rhodopsin exhibits about 2 times more efficient G protein activation as compared with cone visual pigments at 20 °C in a poikilothermic animal (carp) (11). Although we used rod G_t α-subunit in the present assay, it has been suggested that rod and cone G_t α-subunits are functionally interconvertible *in vivo* and *in vitro* (39–41).

Contribution of G_t Activation Efficiencies of Visual Pigments to Photoresponses of Rods and Cones—Electrophysiological analyses indicated that the amplification efficiency for the single photon response of rods of wild-type mice was about 3-fold greater than that of mG knock-in mice (7). This difference is explained by the difference in V_{max}/R* of G_t activation between mRh and mG at 37 °C. In the previous studies, the amplification efficiency of the transduction cascade per bleached pigment in mouse rods was about 6.8-fold higher than that in mouse cones (7, 8). Taken together, that finding combined with the present results suggests that about half of the difference in signal amplification between rods and cones is caused by the difference between the G_t activation efficiencies of rhodopsin and cone visual pigments. We confirmed that the native rod membrane environment can be mimicked by the method using POPC/POPG nanodiscs. However, we cannot completely exclude the possibility that G_t activation efficiency of the reconstituted cone visual pigments in nanodiscs is different from that of the cone visual pigments in native cone membranes because the lipid composition of nanodiscs (POPC/POPG) was different from that in the native cone membranes. It is extremely hard at the present time to isolate cone outer segments containing mG from rod outer segments in mouse retinas because about 98% of photoreceptor cells in the retinas are rod photoreceptor cells. Also, it is impracticable to isolate lipids from cone outer segments to prepare nanodisc containing native lipids. Therefore, we have tried to estimate the effect of lipid composition on the G_t activation efficiency. Yuan *et al.* (42) reported that the lipid composition of gecko photoreceptor outer segment membranes that contain cone-type pigments contained more negatively charged and unsaturated phospholipids than rods. Therefore, we prepared nanodisc sample containing only POPC and that containing the mixture of DOPC and POPG at a ratio of 3:2 (DOPC/POPG) to change the contents of negative charges and unsaturation of the lipids and measure G_t activation efficiencies of bvRh and mG (Fig. 5 and Table 2). The results indicated that the G_t activation efficiencies of bvRh and mG are independent of lipid composition, confirming that the difference in G_t activation efficiency between rhodopsin and cone visual pigments is lipid-independent. However, it was also reported that the amplitude of the single photon response of *Xenopus* rods in which human or salamander red-sensitive cone visual pigment was expressed was similar (less than a 2-fold difference) to that of *Xenopus* rods in which *Xenopus* or human rhodopsin was expressed (43). The discrepancy between that report and our present findings could be due to the difference in the temperature of measurements or to the presence of A2 retinal in the *Xenopus* retina. Therefore, in the future, it will be important to measure the G_t activation efficiencies of *Xenopus* and human rhodopsin and human and salamander red-sensitive cone visual pigments reconstituted with A2 retinal at about 20 °C by using nanodisc samples.

G_t-activating States of Rhodopsin and Cone Visual Pigments—To characterize the G_t-activating state (Meta-II) of rhodopsin and cone visual pigments, we analyzed their photobleaching processes and estimated $F_{\text{Meta-II}}$ in their equilibrium states in POPC/POPG nanodiscs (Tables 3 and 4). The specific G_t activation efficiency of Meta-II (V_{max}/MII) was calculated using V_{max}/R* and $F_{\text{Meta-II}}$. V_{max}/MII of rhodopsin was greater than those of cone visual pigments (Table 1 and Fig. 8), which was also consistent with the different amplification efficiency between rods and cones.

In all the experiments presented here, bovine rod G_t was used. Although V_{max}/MII of bvRh was greater than that of cG, the amino acid residues of the second and third cytoplasmic loops of both pigments, which interact with G_t (44), are well conserved. Thus, it is suggested that the different G_t activation efficiencies of rhodopsin and cone visual pigments derive from differences of the conformation of their Meta-II complex with G_t. Arrhenius plots (Fig. 8) indicated that the activation energy (E_a) of cone visual pigments was about 2-fold greater than that of rhodopsin. This implies that the activation of G_t by Meta-II of cone visual pigments requires greater enthalpy than that by Meta-II of rhodopsin. These findings suggest that there is some difference in the hydrogen bond(s) and/or hydrophobic bond(s) involved in the interaction between G_t and Meta-II.

Properties of Different Subtypes of Cones—Our analysis found not only a difference in G_t activation efficiencies between rhodopsin and cone visual pigments but also a difference between different subtypes of cone visual pigments (cG and mG). $F_{\text{Meta-II}}$ of mG (L group) was smaller than that of cG (M2 group), and thus V_{max}/R* of mG was lower than that of cG at 37 °C, although their V_{max}/MII values were comparable. The photoresponses of M-cones and S-cones in mouse are very similar but not identical (8). Because the subtypes of G_t, phosphodiesterase, and other functional proteins are the same in cones, it is likely that the different photoresponses among cones mainly depend on the different molecular properties of cone visual pigments. The molecular basis of the photoresponses of cones will be clarified by further analyses of the molecular properties of functional proteins, including visual pigments in nanodiscs.

In summary, we showed differences in the G_t activation efficiencies of rhodopsin and cone visual pigments using nanodiscs that mimic the native membrane environment. The difference in G_t activation efficiencies between rhodopsin and cone visual pigments is quantitatively consistent with the different amplification efficiency between rods and cones. The specific G_t activating efficiency of the active state of rhodopsin is greater than that of cone visual pigments. Rhodopsin appears to have acquired these molecular properties of its active state during the process of its evolution from a cone visual pigment to increase its G protein activation efficiency.

Acknowledgments—We thank Dr. S. Koike for providing us with HEK293T cell lines and Prof. R. S. Molday for the generous gift of a Rho1D4-producing hybridoma. We are also grateful to Dr. Elizabeth Nakajima and Take Matsuyama for critical reading of our manuscript and invaluable comments.

REFERENCES

1. Fu, Y., and Yau, K. W. (2007) Phototransduction in mouse rods and cones. *Pflugers Arch.* **454,** 805–819
2. Kawamura, S., and Tachibanaki, S. (2008) Rod and cone photoreceptors: molecular basis of the difference in their physiology. *Comp. Biochem. Physiol. A Mol. Integr. Physiol.* **150,** 369–377
3. Yau, K. W. (1994) Phototransduction mechanism in retinal rods and cones. The Friedenwald Lecture. *Invest. Ophthalmol. Vis. Sci.* **35,** 9–32
4. Ebrey, T., and Koutalos, Y. (2001) Vertebrate photoreceptors. *Prog. Retin. Eye Res.* **20,** 49–94
5. Arshavsky, V. Y., Lamb, T. D., and Pugh, E. N., Jr. (2002) G proteins and phototransduction. *Annu. Rev. Physiol.* **64,** 153–187
6. Shichida, Y., and Imai, H. (1998) Visual pigment: G-protein-coupled receptor for light signals. *Cell. Mol. Life Sci.* **54,** 1299–1315
7. Sakurai, K., Onishi, A., Imai, H., Chisaka, O., Ueda, Y., Usukura, J., Nakatani, K., and Shichida, Y. (2007) Physiological properties of rod photoreceptor cells in green-sensitive cone pigment knock-in mice. *J. Gen. Physiol.* **130,** 21–40
8. Nikonov, S. S., Kholodenko, R., Lem, J., and Pugh, E. N., Jr. (2006) Physiological features of the S- and M-cone photoreceptors of wild-type mice from single-cell recordings. *J. Gen. Physiol.* **127,** 359–374
9. Fukada, Y., Okano, T., Artamonov, I. D., and Yoshizawa, T. (1989) Chicken red-sensitive cone visual pigment retains a binding domain for transducin. *FEBS Lett.* **246,** 69–72
10. Imai, H., Terakita, A., Tachibanaki, S., Imamoto, Y., Yoshizawa, T., and Shichida, Y. (1997) Photochemical and biochemical properties of chicken blue-sensitive cone visual pigment. *Biochemistry* **36,** 12773–12779
11. Tachibanaki, S., Yonetsu, S., Fukaya, S., Koshitani, Y., and Kawamura, S. (2012) Low activation and fast inactivation of transducin in carp cones. *J. Biol. Chem.* **287,** 41186–41194
12. Tachibanaki, S., Tsushima, S., and Kawamura, S. (2001) Low amplification and fast visual pigment phosphorylation as mechanisms characterizing cone photoresponses. *Proc. Natl. Acad. Sci. U.S.A.* **98,** 14044–14049
13. Shi, G., Yau, K. W., Chen, J., and Kefalov, V. J. (2007) Signaling properties of a short-wave cone visual pigment and its role in phototransduction. *J. Neurosci.* **27,** 10084–10093
14. Denisov, I. G., Grinkova, Y. V., Lazarides, A. A., and Sligar, S. G. (2004) Directed self-assembly of monodisperse phospholipid bilayer Nanodiscs with controlled size. *J. Am. Chem. Soc.* **126,** 3477–3487
15. Ritchie, T. K., Grinkova, Y. V., Bayburt, T. H., Denisov, I. G., Zolnerciks, J. K., Atkins, W. M., and Sligar, S. G. (2009) Chapter 11—reconstitution of membrane proteins in phospholipid bilayer nanodiscs. *Methods Enzymol.* **464,** 211–231
16. Kuszak, A. J., Pitchiaya, S., Anand, J. P., Mosberg, H. I., Walter, N. G., and Sunahara, R. K. (2009) Purification and functional reconstitution of monomeric μ-opioid receptors: allosteric modulation of agonist binding by Gi2. *J. Biol. Chem.* **284,** 26732–26741
17. Bayburt, T. H., and Sligar, S. G. (2010) Membrane protein assembly into nanodiscs. *FEBS Lett.* **584,** 1721–1727
18. Whorton, M. R., Jastrzebska, B., Park, P. S., Fotiadis, D., Engel, A., Palczewski, K., and Sunahara, R. K. (2008) Efficient coupling of transducin to monomeric rhodopsin in a phospholipid bilayer. *J. Biol. Chem.* **283,** 4387–4394
19. Bayburt, T. H., Leitz, A. J., Xie, G., Oprian, D. D., and Sligar, S. G. (2007) Transducin activation by nanoscale lipid bilayers containing one and two rhodopsins. *J. Biol. Chem.* **282,** 14875–14881
20. Tsukamoto, H., Sinha, A., DeWitt, M., and Farrens, D. L. (2010) Monomeric rhodopsin is the minimal functional unit required for arrestin binding. *J. Mol. Biol.* **399,** 501–511
21. Bayburt, T. H., Vishnivetskiy, S. A., McLean, M. A., Morizumi, T., Huang, C. C., Tesmer, J. J., Ernst, O. P., Sligar, S. G., and Gurevich, V. V. (2011) Monomeric rhodopsin is sufficient for normal rhodopsin kinase (GRK1) phosphorylation and arrestin-1 binding. *J. Biol. Chem.* **286,** 1420–1428
22. Whorton, M. R., Bokoch, M. P., Rasmussen, S. G., Huang, B., Zare, R. N., Kobilka, B., and Sunahara, R. K. (2007) A monomeric G protein-coupled receptor isolated in a high-density lipoprotein particle efficiently activates its G protein. *Proc. Natl. Acad. Sci. U.S.A.* **104,** 7682–7687
23. Okano, T., Kojima, D., Fukada, Y., Shichida, Y., and Yoshizawa, T. (1992) Primary structures of chicken cone visual pigments: vertebrate rhodopsins have evolved out of cone visual pigments. *Proc. Natl. Acad. Sci. U.S.A.* **89,** 5932–5936
24. Yokoyama, S. (2008) Evolution of dim-light and color vision pigments. *Annu. Rev. Genomics Hum. Genet.* **9,** 259–282
25. Shichida, Y., and Matsuyama, T. (2009) Evolution of opsins and phototransduction. *Philos. Trans. R. Soc. Lond. B Biol. Sci.* **364,** 2881–2895
26. Morizumi, T., Imai, H., and Shichida, Y. (2003) Two-step mechanism of interaction of rhodopsin intermediates with the C-terminal region of the transducin α-subunit. *J. Biochem.* **134,** 259–267
27. Sato, K., Yamashita, T., Imamoto, Y., and Shichida, Y. (2012) Comparative studies on the late bleaching processes of four kinds of cone visual pigments and rod visual pigment. *Biochemistry* **51,** 4300–4308
28. Kuwayama, S., Imai, H., Morizumi, T., and Shichida, Y. (2005) Amino acid residues responsible for the meta-III decay rates in rod and cone visual pigments. *Biochemistry* **44,** 2208–2215
29. Banerjee, S., Huber, T., and Sakmar, T. P. (2008) Rapid incorporation of functional rhodopsin into nanoscale apolipoprotein bound bilayer (NABB) particles. *J. Mol. Biol.* **377,** 1067–1081
30. Imamoto, Y., Seki, I., Yamashita, T., and Shichida, Y. (2013) Efficiencies of activation of transducin by cone and rod visual pigments. *Biochemistry* **52,** 3010–3018
31. Imamoto, Y., and Shichida, Y. (2008) Thermal recovery of iodopsin from photobleaching intermediates. *Photochem. Photobiol.* **84,** 941–948
32. Tachibanaki, S., Imai, H., Mizukami, T., Okada, T., Imamoto, Y., Matsuda, T., Fukada, Y., Terakita, A., and Shichida, Y. (1997) Presence of two rhodopsin intermediates responsible for transducin activation. *Biochemistry* **36,** 14173–14180
33. Anderson, R. E., and Maude, M. B. (1970) Phospholipids of bovine outer segments. *Biochemistry* **9,** 3624–3628
34. Albert, A. D., Young, J. E., and Paw, Z. (1998) Phospholipid fatty acyl spatial distribution in bovine rod outer segment disk membranes. *Biochim. Biophys. Acta* **1368,** 52–60
35. Tsukamoto, H., Szundi, I., Lewis, J. W., Farrens, D. L., and Kliger, D. S. (2011) Rhodopsin in nanodiscs has native membrane-like photointermediates. *Biochemistry* **50,** 5086–5091
36. Sato, K., Morizumi, T., Yamashita, T., and Shichida, Y. (2010) Direct observation of the pH-dependent equilibrium between metarhodopsins I and II and the pH-independent interaction of metarhodopsin II with transducin C-terminal peptide. *Biochemistry* **49,** 736–741
37. Morizumi, T., Imai, H., and Shichida, Y. (2005) Direct observation of the complex formation of GDP-bound transducin with the rhodopsin intermediate having a visible absorption maximum in rod outer segment membranes. *Biochemistry* **44,** 9936–9943

38. Matsuyama, T., Yamashita, T., Imamoto, Y., and Shichida, Y. (2012) Photochemical properties of mammalian melanopsin. *Biochemistry* **51,** 5454–5462
39. Deng, W. T., Sakurai, K., Liu, J., Dinculescu, A., Li, J., Pang, J., Min, S. H., Chiodo, V. A., Boye, S. L., Chang, B., Kefalov, V. J., and Hauswirth, W. W. (2009) Functional interchangeability of rod and cone transducin α-subunits. *Proc. Natl. Acad. Sci. U.S.A.* **106,** 17681–17686
40. Gopalakrishna, K. N., Boyd, K. K., and Artemyev, N. O. (2012) Comparative analysis of cone and rod transducins using chimeric Gα subunits. *Biochemistry* **51,** 1617–1624
41. Mao, W., Miyagishima, K. J., Yao, Y., Soreghan, B., Sampath, A. P., and Chen, J. (2013) Functional comparison of rod and cone Gα_t on the regulation of light sensitivity. *J. Biol. Chem.* **288,** 5257–5267
42. Yuan, C., Chen, H., Anderson, R. E., Kuwata, O., and Ebrey, T. G. (1998) The unique lipid composition of gecko (Gekko Gekko) photoreceptor outer segment membranes. *Comp. Biochem. Physiol. B Biochem. Mol. Biol.* **120,** 785–789
43. Kefalov, V., Fu, Y., Marsh-Armstrong, N., and Yau, K. W. (2003) Role of visual pigment properties in rod and cone phototransduction. *Nature* **425,** 526–531
44. König, B., Arendt, A., McDowell, J. H., Kahlert, M., Hargrave, P. A., and Hofmann, K. P. (1989) Three cytoplasmic loops of rhodopsin interact with transducin. *Proc. Natl. Acad. Sci. U.S.A.* **86,** 6878–6882
45. Tachibanaki, S., Imai, H., Terakita, A., and Shichida, Y. (1998) Identification of a new intermediate state that binds but not activates transducin in the bleaching process of bovine rhodopsin. *FEBS Lett.* **425,** 126–130